Proceedings of the ASME 2017 36th International Conference on Ocean, Offshore and Arctic Engineering
OMAE2017
June 25-30, 2017, Trondheim, Norway

OMAE2017-61130

ANALYSIS OF FAILURE MECHANISMS IN SILICA AND CARBONATE SANDS BENEATH A STRIP FOUNDATION UNDER VERTICAL LOADING

Yining Teng
Centre for Offshore Foundation Systems
The University of Western Australia
Perth, WA, Australia

Sam Stanier
Centre for Offshore Foundation Systems
The University of Western Australia
Perth, WA, Australia

Susan Gourvenec
Centre for Offshore Foundation Systems
The University of Western Australia
Perth, WA, Australia

ABSTRACT

This paper reports the deformation behavior of silica and carbonate sands under a strip foundation subjected to uniaxial vertical load. Small-scale physical modelling tests of a strip surface foundation under vertical load were conducted in a geotechnical centrifuge and Particle Image Velocimetry/Digital Image Correlation (PIV/DIC) was used to analyze images of an exposed plane of the model beneath the foundation to visualize the failure mechanisms. The observed mechanisms are interpreted in conjunction with load-settlement response and cone penetrometer resistance profiles. The failure mechanisms are illustrated through normalized vertical and horizontal displacement fields and shear and volumetric strain fields derived from the PIV analysis. Different soil deformation mechanisms and load-settlement responses were observed in the different sands. Soil resistance profiles measured using a miniature cone penetrometer do not correlate with the measured foundation bearing resistance and an interpretation of particle shape effect is introduced to explain the differing behaviors. The results presented improve understanding of the different responses in carbonate sands and silica sand beneath a shallow foundation under vertical load.

Keywords: Failure mechanism, shallow foundation, carbonate sands, PIV, DIC

NOMENCLATURE

B	width of foundation
C_u	coefficient of uniformity
D_{50}	mean particle size
D_r	relative density
e_{max}	maximum void ratio
e_{min}	minimum void ratio
L	length of foundation
q	bearing pressure
q_c	cone resistance
R	roundness of particle
S	sphericity of particle
w	foundation displacement
x	horizontal position
z	penetration depth

INTRODUCTION

Conventional bearing capacity theory for shallow foundations is based on analytical solutions of a general shear failure mechanism (Terzaghi 1943), which is very commonly seen in silica sands. Different failure mechanisms in carbonate sands may lead to discrepancies in soil property interpretation and foundation bearing capacity analysis. Differences in compressibility of a range of carbonate sands, compared to siliceous materials have been reported (Coop 1990); differences in load-settlement response of shallow foundations on carbonate sands compared to silica sands have been reported (Finnie & Randolph 1994); and different kinematic failure mechanisms in carbonate sands compared to silica sands have been indicated by

finite element analysis (Yamamoto et al. 2008) and observed experimentally (Dijkstra et al. 2013). Different deformation mechanisms or failure modes in sands may result in very different foundation load-displacement response. Experimental observations of the kinematic mechanisms in carbonate sands beneath shallow foundations under vertical load are sparse in the literature. The study presented in this paper contributes data to reduce this knowledge gap.

This paper presents observations from centrifuge model tests, i.e. at prototype stress levels, of shallow foundation response in a silica and two carbonate sands under vertical loading. The samples are characterized by their relative density and through miniature cone penetrometer tests (CPT). Load-settlement response of the foundations is reported along with observations of the failure mechanisms using a Particle Image Velocimetry/ Digital Image Correlation (PIV/DIC) technique (Stanier et al. 2015).

EXPERIMENTAL DETAILS

Methodology

Physical modelling tests using Particle Image Velocimetry/ Digital Image Correlation (PIV/DIC) have been conducted in the 1.8 m radius beam centrifuge at the University of Western Australia (UWA).

Figure 1 shows a schematic of PIV test set-up. A strip mat foundation (model size: $B \times L$: 50 mm × 100 mm; prototype size: 2.5 m × 5 m) was placed in the centre of a strongbox with an acrylic window on one face. The foundation was loaded centrically and vertically at a constant vertical displacement rate of 0.05mm/s until the foundation bearing resistance reached the capacity of the load cell. Cone penetrometer tests (CPT) were conducted to characterize the shear strength sample.

Hardware

The hardware used in the testing programme included:

- Centrifuge strongbox – a 650 × 390 × 325 mm steel box housing the camera, lighting and PIV strongbox.
- PIV strongbox – a 340 × 100 × 300 mm steel box housing the sand sample for testing, fitted with a transparent acrylic window to enable image recording of the sand face.
- Camera – mounted to capture the whole exposed cross-section of the model. A 5-megapixel camera allowing a maximum frame rate of 15 frame/s at full resolution was used (Allied Vision Tech. Prosilica GC2450C).
- LED panels (CCS Industries Ltd. LDL2-266X30SW-WD) – used to achieve bright and even lighting on the testing section.
- Control unit – to drive and control the camera and LED panels. Frame rate and exposure time of the camera, and light intensity of LED panels are controllable.
- Model strip foundation – fabricated from anodized aluminum with smooth surface. The foundation extends the full width of the PIV strongbox to replicate an infinitely long strip foundation.
- Load cell – an in-house column load cell with load capacity of 8 kN. Used to measure the axial load applied to the foundation. Mounted between the foundation and the actuator.

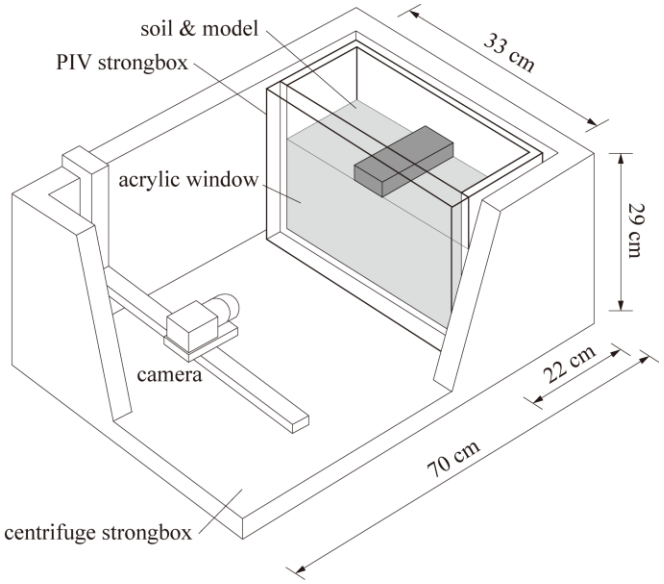

Figure 1. Schematic of centrifuge PIV test set-up.

The PIV hardware and interpretation methods have previously been described in detail in White et al. (2003) and Stanier et al. (2013). The foundation displacement is controlled by an in-house motion control system (De Catania et al., 2010). Data acquisition of loads and displacements was achieved using an in-house data acquisition system (Gaudin et al., 2009).

A MATLAB based PIV/DIC software package, GeoPIV-RG (Stanier et al., 2015) is used. GeoPIV-RG – incorporating a first-order subset shape function, bi-quintic b-spline image intensity interpolation and IC-GN subset deformation parameter optimization – was used to achieve high measurement precision. The software can be freely downloaded from the GeoPIV-RG website (http://www. geopivrg.com).

Soil sample and soil properties

A coarse silica sand (CS) and two carbonate sands, Ledge Point carbonate sand (LP) and Legendre carbonate sand (LGD), were tested in this investigation. The CS sand is a commercial silica sand with broadly uniform grain shape, manufactured by Sibelco Group, Australia. The LP carbonate sand was collected from a coastal location in Western Australia, and has very high calcium carbonate content, including organic remains, and angular particles. The LGD carbonate sand was recovered from the seabed at the Legendre field on the North West Shelf offshore Western Australia, and has a more rounded shape than the LP carbonate sand. Particle size distributions of the samples were obtained by sieving and are shown in Figure 2. The measured

soil properties of the samples are listed in Table 1. The D_{50} of CS sand, LP sand and LGD sand are 0.51mm, 0.21mm and 1.05mm, respectively; and all samples are poorly graded with low coefficient of uniformity, C_u.

Scanning Electron Microscopy (SEM) was carried out to identify shape characteristics of the grains of each of the sands. The SEM images are shown in Figure 3 at two consistent scales for all three sands. Visually, each sand has clearly different particle characteristics. The carbonate sands (LP, LGD) are more angular and variable in shape compared to the coarse silica sand, which has uniform and rounded particles. Particle shape effect will be addressed later in this paper.

Cone penetrometer tests were conducted to estimate the soil strength of the sand samples. Figure 4 presents the measured cone tip resistance for the three sands in free-field sites. The Legendre (LGD) carbonate sand generated the highest cone penetrometer resistance followed by Ledge Point (LP) carbonate sand, whilst the coarse silica (CS) sand yielded the lowest resistance.

Table 1. Material properties of sand samples

Sand	e_{max} (-)	e_{min} (-)	D_r (%)	D_{50} (mm)	C_u (-)
Coarse silica (CS)	0.69	0.54	70	0.51	1.38
Ledge Point (LP) carbonate sand	1.17	0.80	47	0.21	2.67
Legendre (LGD) carbonate sand	0.84	0.51	71	1.05	2.09

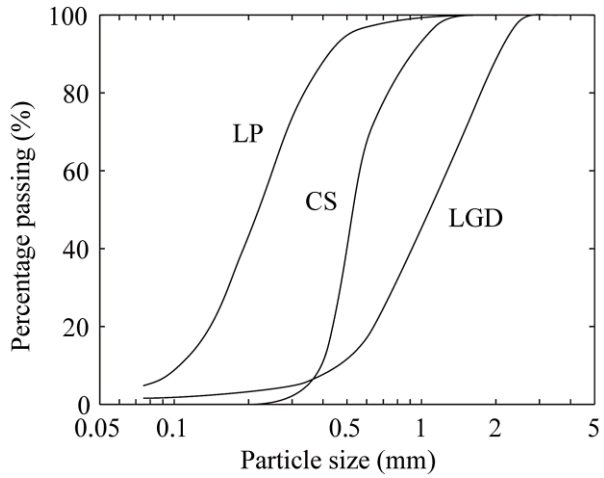

Figure 2. Particle size distribution: (CS) coarse silica sand; (LP) Ledge Point carbonate sand; (LGD) Legendre carbonate sand.

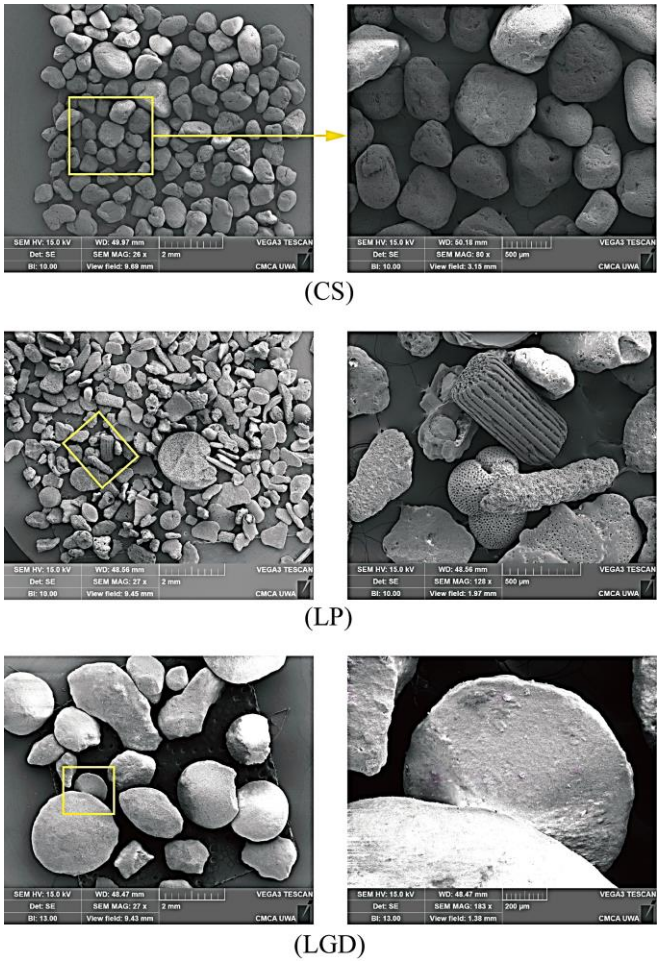

Figure 3. Scanning electron microscopy (SEM): (CS) coarse silica sand; (LP) Ledge Point carbonate sand; (LGD) Legendre carbonate sand.

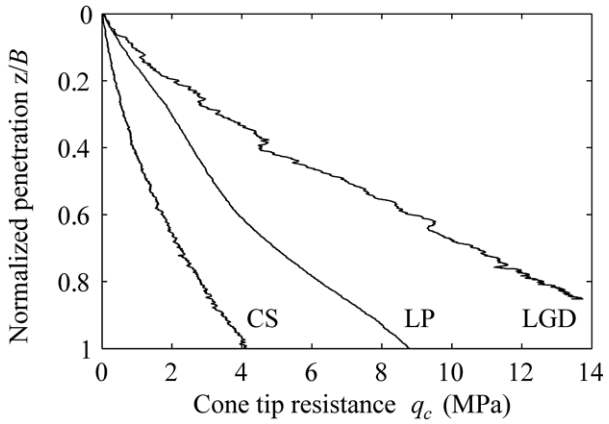

Figure 4. Cone penetrometer resistance: (CS) coarse silica sand; (LP) Ledge Point carbonate sand; (LGD) Legendre carbonate sand.

FOUNDATION TEST RESULTS

Load-displacement response

Figure 5 shows the foundation bearing pressure profiles measured in the three sands. The Legendre carbonate sand (LGD) exhibits the highest bearing pressures, as in the cone penetration tests. However, contrary to the cone penetration tests the Ledge Point carbonate sand exhibits the lowest bearing pressures. Particle crushing was not visually observed during loading of the foundations for any of the sand samples.

Differences in mobilised bearing pressure at a particular normalized penetration depth can be quite significant. For example, at a normalized displacement of 4% of the foundation width, the bearing pressure in the Legendre sand is double that recorded in the Ledge Point sand. Considering a constant bearing pressure, e,g, 200 kPa, the settlement ranges by a factor of two. The practical implication is that the same foundation, with a given operative vertical load, would settle significantly different amounts on different sediments. Understanding whether differing failure mechanism or soil properties cause this variation in load-settlement response, is important to developing reliable design guidance. Visualization of the failure mechanisms, through Particle Image Velocimetry (PIV), can contribute to this understanding.

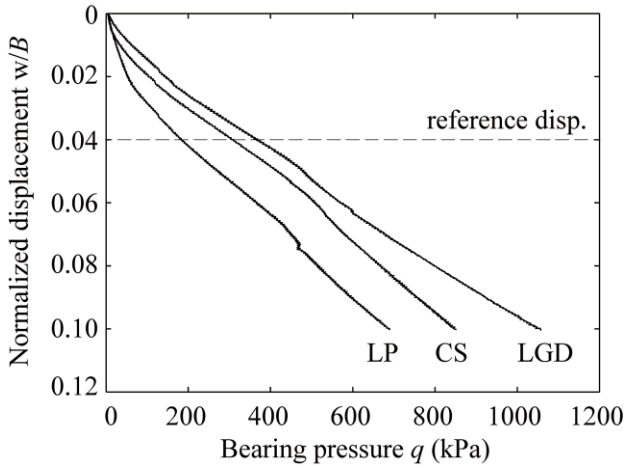

Figure 5. Bearing pressure measured in foundation tests: (CS) coarse silica sand; (LP) Ledge Point carbonate sand; (LGD) Legendre carbonate sand.

PIV results

Figure 6 compares displacement vector fields with normalized horizontal (LHS) and vertical (RHS) displacement contours (normalized by the foundation displacement) for each of the sands at a normalized displacement, w/*B*, of 4%. This visualization illustrates whether horizontal or vertical soil displacements dominate the mechanism mobilised for each of the sands. The displacement fields are clearly very different for the carbonate sands (LP, LGD) when compared to the silica sand (CS). There is significantly more lateral displacement in the

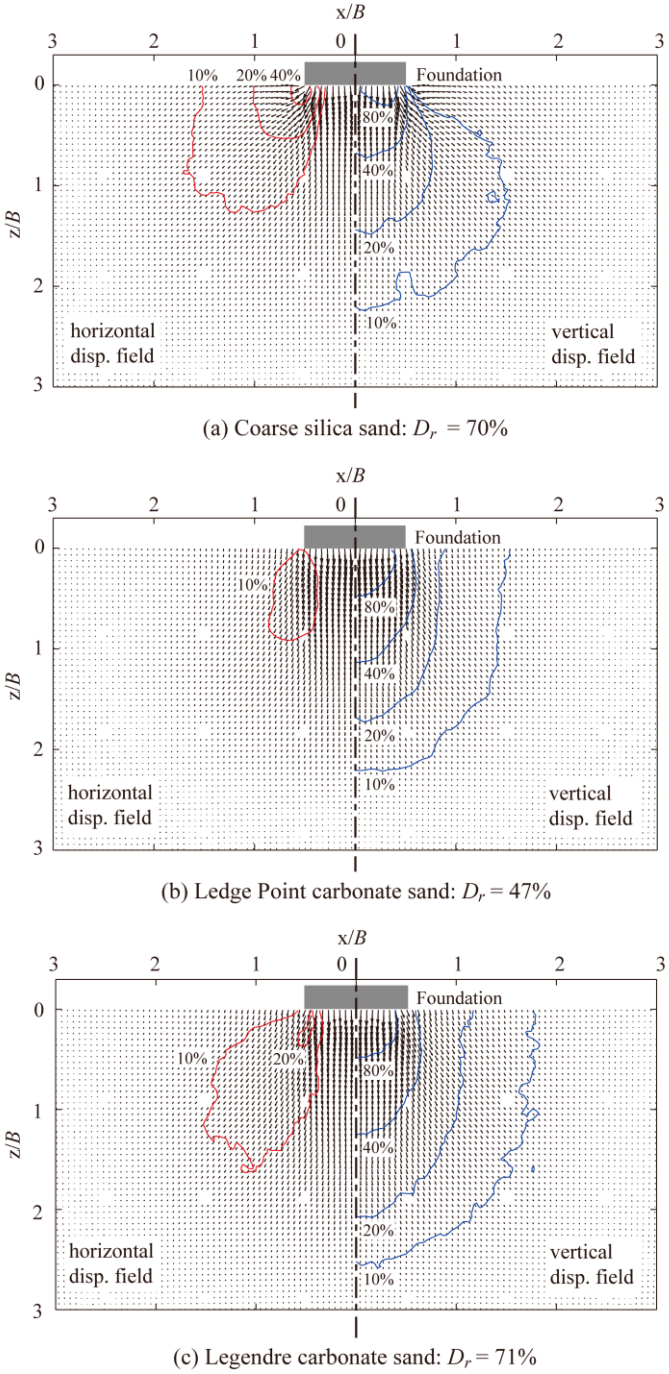

Figure 6. Normalized horizontal displacement contour field (left) and mirrored corresponding vertical displacement contour field (right). Soil displacements normalized by applied foundation displacement.

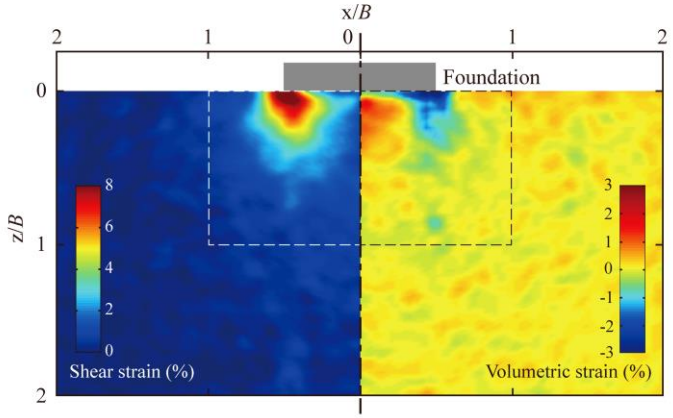

(a) Coarse silica sand: D_r = 70%

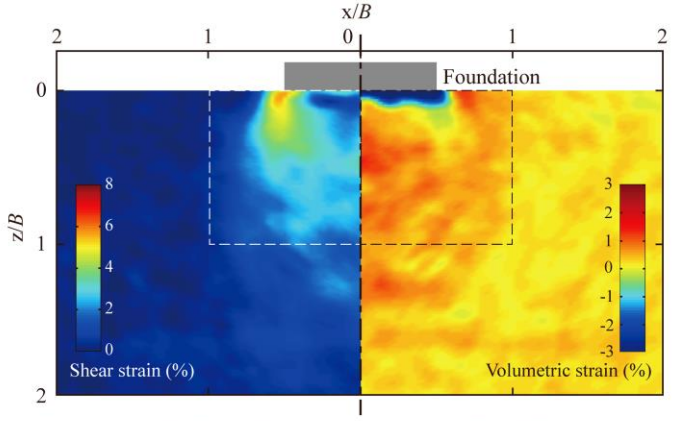

(b) Ledge Point carbonate sand: D_r = 47%

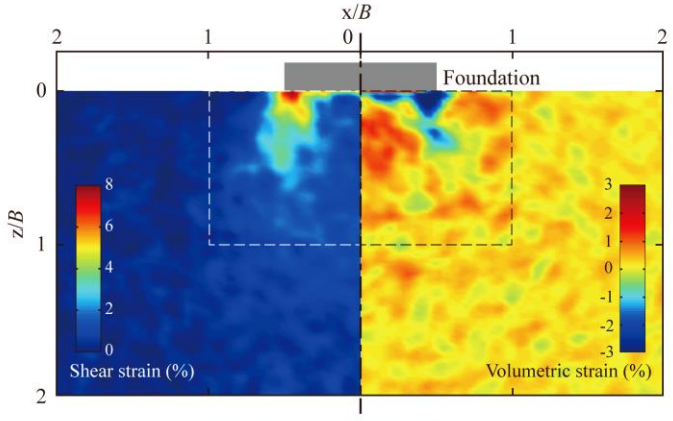

(c) Legendre carbonate sand: D_r = 71%

Figure 7. Normalized shear strain field (left) and mirrored corresponding volumetric strain field (right). Shear strain and volumetric strain expressed as percentage.

silica sand (CS) than in either of the carbonate sands where vertical displacement (settlement) tends to dominate. This is indicative that a 'punching shear' type failure mechanism is dominant in carbonate sands.

Strain fields, derived from the displacement fields, are plotted in Figure 7 to further explore the difference in failure mechanisms. Shear strain fields are shown on the left side of the figures with corresponding volumetric strain fields for the same region mirrored on the right side. Sign convention is compression-positive for the volumetric strain field. In the coarse silica sand a highly concentrated zone of shearing is seen at the corner of the foundation. For the carbonate sands the shear strain fields are more diffuse and of generally lower magnitude. In the volumetric strain fields, there appears to be a dilating zone immediately beneath the foundation in all tests, however there is significantly more volumetric compression beneath the foundation in the carbonate sand tests (LP, LGD) than the silica sand test (CS), which agrees well with the difference in mechanisms seen in Figure 6.

EFFECT OF PARTICLE SHAPE

In this section, the effect of particle shape on the foundation failure mechanisms is considered. Two measures of particle characteristic, sphericity and roundness, have been estimated for each of the sands using the SEM images (shown in Figure 3):

1. Sphericity *S*: The sphericity of a particle is the ratio of its largest inscribed sphere relative to the diameter of its smallest circumscribed sphere. Sphericity refers to the 3D global particle shape reflecting the similarity between the particle's length, height and width.

2. Roundness *R*: The roundness of a particle is measured using its maximum projected area, defined as the ratio of the average radius of the area relative to the maximum inscribed circle of the

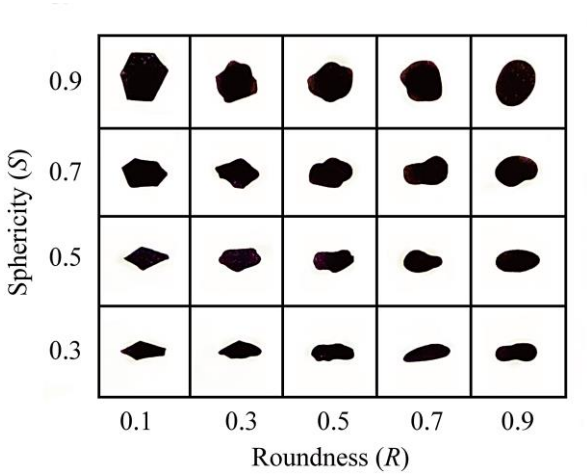

Figure 8. Chart for particle shape visual estimation: Sphericity (S) and roundness (R). (after Krumbein & Sloss, 1964)

area. Roundness describes the 2D major surface features of the particle.

A reference for visual estimation of sphericity and roundness is adapted from Krumbein & Sloss (1963) in Figure 8.

The particle shape parameter estimates for the sands considered in this study are summarised in Table 2. The coarse silica (CS) sand is rounded and uniform with very high sphericity and roundness at ~ 0.9. The particle shapes of LP carbonate sand are mostly irregular and highly angular. The average sphericity and roundness of LP carbonate sand are all very low at ~ 0.3. The LGD carbonate sand is more rounded than the LP sand. Disk shape and blade shape particles are common in LGD sand. The sphericity and roundness of LGD sand are estimated as ~ 0.5 and ~ 0.7 respectively.

Table 2. Estimates of particle shape parameters

Sand	Sphericity S (-)	Roundness R (-)
coarse silica (CS)	~0.9 (high)	~0.9 (high)
Ledge Point (LP) carbonate sand	~0.3 (low)	~0.3 (low)
Legendre (LGD) carbonate sand	~0.5 (med)	~0.7 (high)

The sphericity, S, and roundness, R, of the particles could explain the different trends of behaviour observed between the foundation and the cone penetrometer penetration resistance, i.e. that the Ledge Point sand exhibited a lower foundation penetration resistance but higher cone resistance than the coarse silica sand.

Sphericity, S, is high in coarse silica sand (0.9), but is relatively low in LGD carbonate sand (0.5) and LP carbonate sand (0.3). It is found that coarse silica sand below the foundation corner has the largest lateral component (40%) of soil displacement under vertical load, followed by LGD sand (20%) and LP sand (10%); c.f. Figure 6 (a, b, c). The sphericity S, as defined previously in the paper, reflects the level of similarity between the particle and its circumscribed sphere. The load transfer between perfectly spherical particles will pass through the centre of each particle. Therefore vertical load can be transferred laterally if two spheres are not aligned vertically, and so the sphericity, S, is likely to influence the direction of load transfer within a volume of particles subjected to non-uniform loads (as in the foundation test). In contrast, for the Ledge Point and Legendre carbonate sand particles, which have lower sphericity, S, the pluviated deposition process adopted in creating the models (similar to natural deposition) is likely to result in the particles being oriented horizontally, causing the load transfer to be predominantly vertical.

The volumetric strain field comparisons (Figure 7) also show that coarse silica sand is the least compressible, followed by LGD carbonate sand and LP carbonate sand, which is the reverse order of the estimated sphericity, S. Cho et al. (2006) summarized a database studying the effect of particle shape on soil properties, which included sphericity, S, roundness, R, and maximum and minimum voids ratios, e_{max} and e_{min}. Table 3 is a reorganized version of the database, sorted with respect to reducing sphericity, S, as the primary target and roundness, R, as the secondary target. When the database is sorted in this way, it shows that most samples with high sphericity and roundness tend to have a smaller range between the maximum and minimum void ratios and therefore less capacity to rearrange under load generating compressive volumetric strains (prior to particle crushing). For the three sands tested in this paper, there is a small range between e_{max} and e_{min} in coarse silica (CS) sand, while the range is much greater in the two carbonate sands (LP, LGD). This observation goes some way to explaining the differences in deformation mechanism observed between the silica and carbonate sands.

Table 3. Database of particle shape information and void ratio (modified from Cho et al. 2006)

Sand sample	Sphericity S (-)	Roundness R (-)	e_{max} (-)	e_{min} (-)
Glass beads	1.00	1.00	0.72	0.54
Ottawa #20/30	0.90	0.90	0.72	0.50
ASTM graded	0.90	0.80	0.82	0.50
ASTM 20/30	0.90	0.80	0.69	—
Michigan Dune	0.87	0.77	0.80	0.56
Nevada	0.85	0.60	0.85	0.57
Ponte Vedra	0.85	0.30	1.07	—
Jekyll Island	0.85	0.30	1.04	—
Ottawa #20/70	0.81	0.76	0.78	0.47
Ticino	0.80	0.40	0.99	0.57
Ottawa #60/80	0.78	0.65	0.85	0.55
Margaret River	0.70	0.70	0.87	—
Ottawa F110	0.70	0.70	0.85	0.54
Daytona Beach	0.70	0.62	1.00	0.64
Sandboil	0.70	0.55	0.79	0.51
Ottawa #45	0.68	0.45	1.10	0.75
Syncrude Tailings	0.62	0.47	1.14	0.59
Ottawa #90	0.60	0.40	1.10	0.73
Blasting	0.55	0.30	1.03	0.70
Fraser River	0.50	0.25	1.13	0.78
Granite powder	0.24	0.40	1.30	0.48

FURTHER WORK

A new synchronized multi-scale PIV methodology enabling analysis of high-resolution 'micro' scale images captured using a second camera and lens with greater magnification has recently been developed (Teng et al. 2016). This system allows the large displacements and strains occurring at the interface of the footing to be measured at a higher resolution, providing further insights

into the differences in response of silica and carbonate sands in qualitative and quantitative ways. Work on the analysis of images captured with the higher resolution camera in a further suite of tests on rectangular foundations on silica and carbonate sands under vertical loading and horizontal cyclic loading is currently in progress at COFS.

CONCLUSIONS

A set of centrifuge model tests have been conducted to investigate the deformation behavior of two carbonate sands and a silica sand beneath a surface strip foundation under monotonic vertical load. Digital images of a cross-section of the model captured continuously during the test were analyzed using PIV, enabling the kinematic mechanisms to be visualized and scrutinized quantitatively in terms of vertical and horizontal components of displacement and shear and volumetric strains. Cone penetrometer tests were used to characterize the samples. Load-settlement responses were observed in the foundation tests that cannot be explained simply from the measured cone resistance. Particle shape is thought to have an impact on the form of deformation mechanisms occurring beneath the foundation – and hence load-settlement response of the foundation. The PIV analyses show a classical general shear mechanism in the silica sand and punching shear mechanism in the carbonate sands. The propensity for these mechanisms to form is thought to be linked to the sphericity, *S*, and roundness, *R* of the sand particles. More rounded particles lead to balanced load spreading in the vertical and horizontal directions whereas the flatter carbonate particles lead to predominantly vertical mechanisms with more expansive zones of volumetric compression. The load-settlement response of the foundation may then be greater than anticipated from conventional interpretation of CPT data based on experience of silica sands. The results presented in this paper have highlighted the potentially complex nature of an apparently simple geotechnical boundary value problem, and provided insights to improve understanding of the load-settlement response of a surface strip foundation on sand under vertical loading.

ACKNOWLEDGMENTS

This work forms part of the activities of the Centre for Offshore Foundation Systems (COFS), which was established in 1997 under the Australian Research Council's Special Research Centres Program. It is currently supported as a node of the Australian Research Council's Centre of Excellence for Geotechnical Science and Engineering, and through the Fugro Chair in Geotechnics, the Lloyd's Register Foundation Chair and Centre of Excellence in Offshore Foundations and the Shell EMI Chair in Offshore Engineering. The second author and the work presented in this paper was supported through ACS grant CE110001009. The authors also acknowledge the facilities, and assistance of the Australian Microscopy & Microanalysis Research Facility at the Centre for Microscopy at UWA.

REFERENCES

Cho, G.C., Dodds, J., & Santamarina, J. C. (2006). Particle shape effects on packing density, stiffness, and strength: natural and crushed sands. *Journal of geotechnical and geoenvironmental engineering, 132*(5), 591-602

Coop, M. R. (1990). The mechanics of uncemented carbonate sands. *Geotechnique, 40*(4), 607-626

De Catania, S., Breen, J., Gaudin, C., & White, D. J. (2010). Development of a multiple axis actuator control system *Proceedings of the Seventh International Conference on Physical Modelling in Geotechnics* (Vol. 1, pp. 325-330).

Dijkstra, J., Gaudin, C., & White, D. J. (2013). Comparison of failure modes below footings on carbonate and silica sands. *International Journal of Physical Modelling in Geotechnics, 13 (1), 2013*

Finnie, I. M., & Randolph, M. F. (1994). Bearing response of shallow foundations in uncemented calcareous soil *Proc., Int. Conf. Centrifuge'94* (pp. 535-540): Balkema Rotterdam, Netherlands.

Gaudin, C., White, D. J., Boylan, N., Breen, J., Brown, T., De Catania, S., & Hortin, P. (2009). A wireless high-speed data acquisition system for geotechnical centrifuge model testing. *Measurement science and technology, 20*(9), 095709

Krumbein, W. C., & Sloss, L. L. (1964). Stratigraphy and sedimentation: JSTOR.

Stanier, S. A., Blaber, J., Take, W. A., & White, D. J. (2015). Improved image-based deformation measurement for geotechnical applications. *Canadian Geotechnical Journal, 53*(5), 727-739

Stanier, S. A., & White, D. J. (2013). Improved image-based deformation measurement in the centrifuge environment

Teng, Y., Stanier, S. A., & Gourvenec, S. M. (2016). Synchronised multi-scale image analysis of soil deformations. *International Journal of Physical Modelling in Geotechnics*, 1-19

Terzaghi, K. (1943). *Theoretical soil mechanics*. London: London : Chapman and Hall.

White, D. J., Take, W. A., & Bolton, M. D. (2003). Soil deformation measurement using particle image velocimetry (PIV) and photogrammetry. *Geotechnique, 53*(7), 619-632

Yamamoto, N., Randolph, M. F., & Einav, I. (2008). Simple formulas for the response of shallow foundations on compressible sands. *International Journal of Geomechanics, 8*(4), 230-239